01 Jan 2023

Modeling Phase Selection And Extended Solubility In Rapid Solidified Alloys

Azeez Akinbo

Yijia Gu
Missouri University of Science and Technology, guyij@mst.edu

Recommended Citation

A. Akinbo and Y. Gu, "Modeling Phase Selection And Extended Solubility In Rapid Solidified Alloys," *Metallurgical and Materials Transactions A: Physical Metallurgy and Materials Science*, Springer; ASM International, Jan 2023.
The definitive version is available at https://doi.org/10.1007/s11661-023-07221-7

ORIGINAL RESEARCH ARTICLE

Modeling Phase Selection and Extended Solubility in Rapid Solidified Alloys

AZEEZ AKINBO and YIJIA GU

A new phase selection model based on the time-dependent nucleation theory was developed to investigate the effect of rapid solidification on extended solubility. The model was applied to predict the solubility as a function of undercooling for several binary Al alloys. The predictions of both eutectic and peritectic systems show good agreement with experimental data. It was demonstrated that the developed model is better than the T_0 line method, which neglected the kinetic process of nucleation. Furthermore, the model can also be applied to ternary and multicomponent phases assuming the nucleation is limited by the scarcest species or the slowest diffuser. The feasibility and reliability of the new model make it a useful tool for novel alloy design for rapid solidification processes such as additive manufacturing.

https://doi.org/10.1007/s11661-023-07221-7

I. INTRODUCTION

IN recent years, the manufacturing community has witnessed a blossom in the research field of 3D printing or additive manufacturing (AM). AM integrates the microscopical material structure synthesis and macroscopic component shaping into one single operation, which promises the direct production of a near-net-shape component with controlled microstructures and properties. In addition, the fusion-based metal AM, which exploited the non-equilibrium process of rapid solidification, enables the development of novel microstructures with extended solubility, reduced partitioning of solute, and refined structures,[1] and opens up a new horizon of microstructure synthesis to achieve exotic properties in alloys. However, due to the large undercooling at the rapidly advancing solidification front, the phase selection in rapid solidification deviates from the equilibrium phase diagram, imposing a significant challenge in the understanding of microstructure development during AM. Even in other well-studied rapid solidification processes, such as liquid metal atomization and melt spinning, understanding the phase selection is still challenging.[2]

One major benefit of the deviated phase selection due to the rapid solidification is the extended solubility. Solid solubility describes the extent of an alloying element dissolved in the matrix solid solution phase without forming another solid phase. It is an important property for alloy development, as it is related to the two major strengthening mechanisms. First, it defines the ceiling of solid solution strengthening. Second, it determines the potential of precipitation strengthening or age hardening, which is one of the most effective strengthening mechanisms for non-ferrous alloys. The maximum solid solubility is found to increase with the cooling rate as well as the undercooling. If all the other solid phases are suppressed by rapid solidification, the matrix phase will become the first to solidify. Thus, the solute atoms that may form other primary solid phases during equilibrium solidification will stay in the matrix phase, and hence the solid solubility of the alloying element is increased. Therefore, rapid solidification processes, including levitation, atomization, melt spinning, and AM, have the potential to extend the maximum solid solubility and fabricate components with unprecedented properties. However, the experimental data on supersaturation are limited to a few alloy systems, and only the maximum solubility is listed.[3,4] Furthermore, the extended solubility is not a fixed value but a function of interface temperature (or undercooling), and it is also affected by the interface velocity.[2] On the experimental side, systematic studies on the dependence of extended solubility on undercooling are very scarce,[2,5] as most recent rapid solidification studies focused on the microstructure formation or phase selection for a given solidification condition (one single undercooling or cooling rate), including levitation,[6–13] atomization,[14] melt spinning,[15–17] and AM.[18–26] Theoretical models of extended solubility are also very scarce, although much progress has been made regarding modeling rapid solidification processes.[27–29] In the

AZEEZ AKINBO, and YIJIA GU are with the Department of Material Science and Engineering, Missouri University of Science and Technology, Rolla MO, 65409. Contact e-mail: yijia.gu@mst.edu.
Manuscript submitted February 19, 2023; accepted October 1, 2023.

Published online: 16 October 2023

following, we briefly discuss the existing models of extended solubility.

To predict the extension of solid solubility in rapid solidification, understanding the mechanism of phase selection is the key. There have been many attempts to model the phase selection and extended solubility in the past a few decades. The phase selection under non-equilibrium condition was first modeled using the so-called T_0 line. The T_0 temperature is defined by the thermodynamic condition that for a given composition c the free energy of the solid phase equals the free energy of the liquid, $G^s(c, T_0) = G^l(c, T_0)$, as shown in Figure 1. Therefore, the T_0 line describes when the diffusionless solidification is thermodynamically allowed.[30] If the Gibbs free energies of the liquid and solid phases of an alloy are known, one can determine maximum solid composition (maximum solid solubility) thermodynamically possible for a given composition at a given temperature.[31] This method determines the maximum possible solid solubility, which can be achieved by complete solute trapping at high enough interfacial velocity. However, this method does not work for peritectic system, since the T_0 line lies on the left side of the solidus as illustrated in Figure 1(b). Later, based on the time-dependent nucleation theory (TDNT), Shao and Tsakiropoulos[32] developed a phase selection model for rapid solidification, which can be used to calculate the extended solubility for both eutectic and peritectic systems. This model was adopted to investigate phase selection and to explain experimental observations in recent AM studies such as selective laser melting (SLM) and electron beam melting (EBM).[18–26] However, this model estimates the diffusivity using viscosity, which may introduce large uncertainty. Additionally, the entropy of fusion used in their work is outdated. Hence, this model has limited capability in predicting the extended solubility for a given composition and undercooling/cooling rate. In addition, how this model is related with T_0 line method has not been studied, except we know that it is from kinetic theory and the other one is purely from thermodynamics.

In this work, we developed a new model based on Shao and Tsakiropoulos's TDNT model by eliminating the kinetic parameters. The new model can be used to predict the phase selection and the associated extended solubility for a given undercooling for both eutectic and peritectic systems. The thermodynamic parameters used in the model can be easily accessed from thermodynamic databases *via* CALPHAD packages, such as Thermo-Calc.[33] and Pandat[34] The model predictions were validated by experimental data. In addition, the model was also extended to ternary system. For eutectic systems, the extended solid solubility was also calculated using the T_0 line and compared with the predictions of the developed model. The result of this work can help explain the appearance of non-equilibrium phases as well as the phenomena related to the extended solubility in rapid solidification processes. In addition, it can be easily adopted to design novel alloys for rapid solidification processes such as fusion-based metal AM.

II. MODEL

Since our new model is developed based on Shao and Tsakiropoulos's model,[32] let us review their work first.

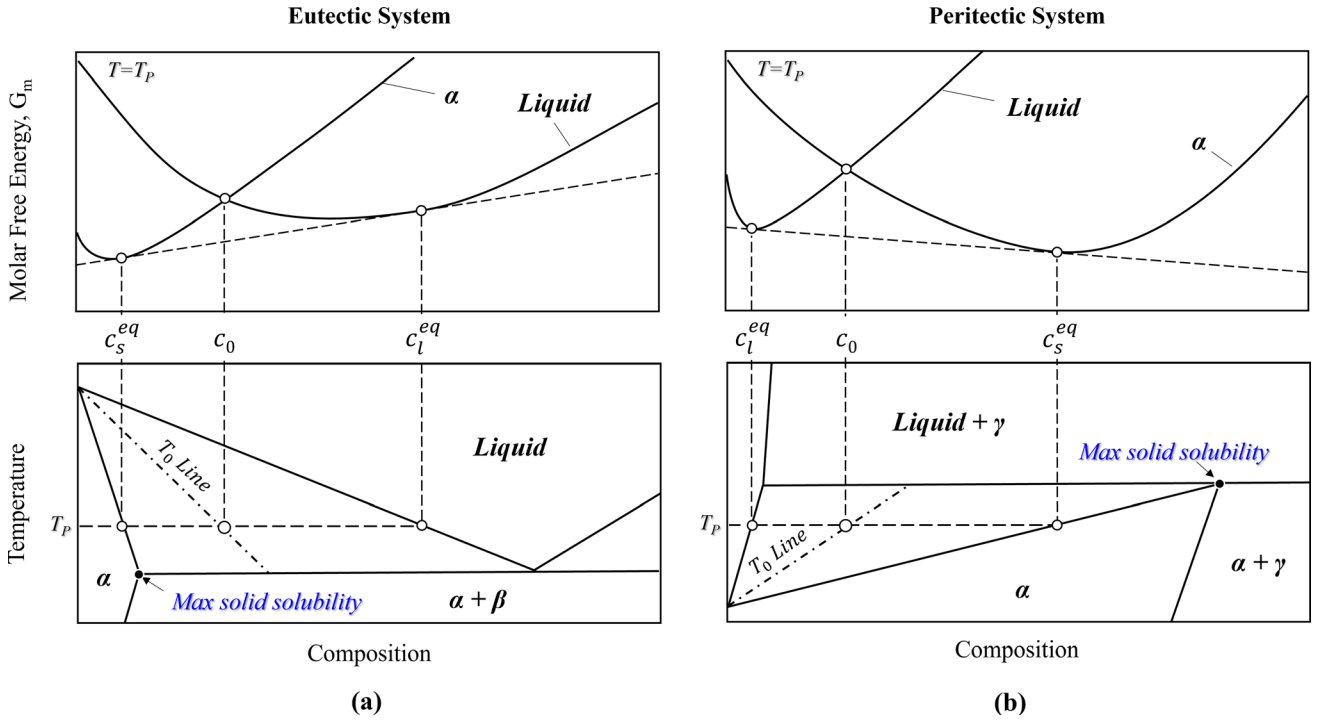

Fig. 1—Schematic phase diagrams and corresponding molar free energies of solid solution α phase and liquid phase at $T = T_P$ for eutectic (*a*) and peritectic system (*b*). c_s^{eq} and c_l^{eq} are equilibrium solid composition and liquid composition at $T = T_P$, respectively.

Based on the time-dependent nucleation theory (TDNT), Shao and Tsakiropoulos derived the incubation time τ as follows (Eq. 14 in the original paper[32]):

$$\tau = \frac{7.2Rf(\theta)}{1-\cos\theta} \cdot \frac{a^4}{x_{\mathrm{L,eff}} d_{\mathrm{a}}^2} \cdot \frac{Tr}{D\Delta S_{\mathrm{m}}\ \Delta T_{\mathrm{r}}^2}, \quad [1]$$

where R is the gas constant, $f(\theta) = \frac{1}{4}(2 - 3\cos\theta + \cos^2\theta)$, θ is the contact angle for heterogeneous nucleation, $T_{\mathrm{r}} = T/T_{\mathrm{M}}$, T is the temperature, T_{M} is the melting temperature of the solid phase, $\Delta T_{\mathrm{r}} = 1 - T_{\mathrm{r}}$, ΔS_{m} is the molar entropy of fusion, a is the atomic jump distance, d_{a} is the average atomic diameter of the solid phase, and $x_{\mathrm{L,eff}}$ is the effective alloy concentration.[32] For a binary A–B system, $x_{\mathrm{L,eff}}$ is taken as $x_{\mathrm{L,A}}/x_{\mathrm{S,A}}$ when the composition of the nucleus is rich in A, where $x_{\mathrm{L,A}}$ and $x_{\mathrm{S,A}}$ stand for molar fraction of A in liquid and solid phases, respectively. The average atomic diameter d_{a} can be calculated from molar weight w_{m} and density ρ of the solid phase *via*

$$d_{\mathrm{a}} = \left(\frac{w_{\mathrm{m}}}{\rho N_0}\right)^{1/3}, \quad [2]$$

where N_0 is the Avogadro's number. To calculate the diffusivity D, Shao and Tsakiropoulos[32] applied the Stokes–Einstein relationship,[35]

$$\frac{\eta D}{T} = \frac{k}{6d_{\mathrm{a,L}}} \quad [3]$$

where η is the viscosity of the melt and $d_{\mathrm{a,L}}$ is the average distance between the liquid atoms and can be taken the same as d_{a} approximately. The above is the original model developed by Shao and Tsakiropoulos in 1994. There has been no further development of the model since. The viscosity η and diffusivity D are kinetic parameters that are not easily accessible. (Although the CALPHAD mobility databases of the major alloy systems are available, they are much less popular than thermodynamic databases and costly.) In the following, we derive our new model that is not dependent on any kinetic parameters.

As η is a function of temperature T only, Eq. [3] gives $Dd_{\mathrm{a}} = kT/6\eta$, which can be regarded the same for all the nucleating phases. Thus, Eq. [1] can be simplified as

$$\tau = c \cdot \frac{1}{x_{\mathrm{L,eff}} d_{\mathrm{a}}} \cdot \frac{T_r}{\Delta S_{\mathrm{m}}\ \Delta T_r^2}, \quad [4]$$

where $c = \frac{43.2f(\theta)a^4\eta}{(1-\cos\theta)N_0 T}$ is the same constant for all the phases.

At the critical temperature T (or the critical undercooling ΔT) when two competing nucleating phases have the same incubation time, we have $\tau_1 = \tau_2$, *i.e.,*

$$\frac{1}{x_{\mathrm{L},1} d_{\mathrm{a}1}} \cdot \frac{T_{r1}}{\Delta S_{\mathrm{m}1}\ \Delta T_{r1}^2} = \frac{1}{x_{\mathrm{L},2} d_{\mathrm{a}2}} \cdot \frac{T_{r2}}{\Delta S_{\mathrm{m}2}\ \Delta T_{r2}^2}, \quad [5]$$

where Z subscripts 1 and 2 stand for the matrix phase and the first solidifying intermetallic phase, respectively, $x_{\mathrm{L},1}$ and $x_{\mathrm{L},2}$ are the effective alloying concentration for each phase. The constant c containing viscosity η is now canceled out. Hence, the model only has the thermodynamic parameters for both competing phases. The thermodynamic parameters, such as $T_{\mathrm{M}1}$, $T_{\mathrm{M}2}$, $\Delta S_{\mathrm{m}1}$, and $\Delta S_{\mathrm{m}2}$, can be assessed from CALPHAD databases. As the density of the solid phase is generally available,[36] the average atomic diameter d_{a} is also accessible using Eq. [2]. Thus, by solving Eq. [5], the critical composition (x_{A}, or solubility limit for the case of a eutectic system) is calculated as a function of temperature T. In other words, for any given temperature T, there is a composition x_{A} when the two competing phases have the same incubation time τ. So, this composition x_{A} is the solubility for this temperature T. Then, the undercooling ΔT is calculated as the difference between the equilibrium liquidus of the alloys system of composition x_{A}, T_{l}, and T, *i.e.,* $\Delta T = T_{\mathrm{l}} - T$. Since each x_{A} corresponds to one ΔT, a diagram of solubility *vs.* undercooling (or a phase diagram of undercooling and composition) can be established. This model is derived based on Shao and Tsakiropoulos's TDNT model,[32] but it does not contain any ambiguous kinetic parameters anymore, which makes the model more feasible and reliable for explaining phase selection in AM and other rapid solidification processes. In "Appendix," we use Al-Cr as an example to show how to use this model to calculate the solubility as a function of undercooling step by step.

III. RESULTS AND DISCUSSION

In this study, we chose Al alloys to test the model considering the availability of experimental data and the importance of extended solubility for strengthening Al alloys. The thermodynamic data obtained from the CALPHAD Al databases, including the entropy of fusion and transition temperature of competing phase, are shown in Table I. It should be noted that the values of entropy of fusion ΔS_{m} assessed from commercial CALPHAD packages are different from Shao and Tsakiropoulos's original work.[32] As the CALPHAD method becomes much more developed over the last a few decades, the thermodynamic data we used here should be more reliable. In the following, we apply the developed model to calculate the phase selection and extended solid solubility for binary eutectic systems (Section III.A), binary peritectic systems (Section III.B), and a ternary system (Section III.C).

A. *Binary Eutectic Systems*

The binary eutectic systems evaluated in this study include Al-Mn, Al-Sc, and Al-Fe. Using the thermodynamic properties of each alloy obtained from CALPHAD packages (Table I), the dependence of the solubility of different alloying elements on undercooling was evaluated using the new model. As shown in Figure 2, depending on the undercooling and the alloy composition, the solid solution α phase is stable on the

upper left of the diagram with higher undercooling and lower alloy composition. In contrast, the intermetallic phase is stable with higher composition and lower undercooling. The phase boundary between α and the intermetallic phase defines the maximum solubility of the alloying element in the solid solution for a given undercooling. It can be seen from the diagrams that the critical undercooling required to suppress the nucleation of the primary intermetallic phase increases with the alloying composition. To achieve higher solid solubility, larger undercooling is required. In the modeling process, several intermetallic phases may be stable and need to be evaluated individually to determine the most stable intermetallic phase. For instance, in Al-Mn systems, Al_6Mn, $Al_{12}Mn$, and other Al-Mn compounds may solidify directly from the liquid. We evaluated the most stable two, Al_6Mn and $Al_{12}Mn$, and plotted them in Figure 2(a). As the Al_6Mn phase boundary lies higher than the $Al_{12}Mn$ phase boundary, it requires more undercooling to suppress Al_6Mn from formation than $Al_{12}Mn$ for any given composition. Therefore, Al_6Mn is the stable intermetallic phase for the binary Al-Mn system. The model predictions of the Al-Mn system were compared with experimental data,[38] which indicates good agreement. The kinks on the calculated phase boundaries correspond to the equilibrium eutectic composition. The Al-Sc binary system, as another eutectic example, was explored. The calculated solid solubility versus undercooling is shown in Figure 2(b).

The maximum solid solubility for a given undercooling in the Al-Mn alloy system was also calculated using the T_0 line method. As shown in Figure 2(a), the solubility calculated using this method shows a similar trend of the solubility dependence on undercooling. However, the predicted solubility is much higher than our model predictions as well as the experimental measurements. This is due to the T_0 line approach being a thermodynamic model in nature, which fails to consider the kinetic nucleation process. Therefore, it defines the theoretical maximum solid solubility that may be impossible to achieve.

B. *Binary Peritectic Systems*

The peritectic forming elements such as Cr and Zr are important dispersoid formers to control the grain structures of Al alloys. However, their solubilities are exceptionally low, which significantly limits the operation window in casting and the following heat treatment. The formation of large primary intermetallic phases such as $Al_{45}Cr_7$ and Al_3Zr in casting is extremely deleterious to mechanical properties such as elongation and fracture toughness. Therefore, increasing the solid solubility of those peritectic forming elements is of great importance to the development of Al alloys.

The binary peritectic systems modeled in this study include Al-Cr, Al-Ti, Al-Zr, and Al-Ta. The diagrams of undercooling against the mass concentration of alloying elements Cr and Zr are shown in Figures 3(a) and (b), respectively. Similar to eutectic systems, the extended solid solubility in peritectic systems is found to increase monotonically with undercooling. In the Al-Cr system, it is found that $Al_{45}Cr_7$ is the stable intermetallic phase, which is consistent with Shao and Tsakiropoulos's work ($Al_{13}Cr_2$).[32] As shown in Figures 3(a) and (b), the model predictions agree well with experimental data by Ichikawa *et al.*[38] It should be emphasized that the parameters used in this work were taken from CALPHAD packages (Table I), and lattice parameters from the literature. None of the parameters are from fitting. Therefore, such good agreements indicate that the developed new model grasps the essence of phase selection and is reliable in the predictions of extended solid solubilities under large undercoolings.

To further understand the dependence of the solid solubility on undercooling, the relationship between the degree of supersaturation (c/c_e) and undercooling of various alloying elements in Al is shown in Figure 4. Supersaturation of the alloying element in the solid solution can be evaluated by comparing each supersaturated solubility c with the maximum solubility of the alloy at equilibrium (c_e).[38] The degree of supersaturation determines the potential of solute species in the matrix phase (α-Al solid solution) to form intermetallic phases. Therefore, it is closely related to the potential of precipitation strengthening. It is also related to the impurity tolerance for elements like Fe and Mn.

The plot shows that the supersaturation degree of eutectic forming elements (Fe, Sc, and Mn) tends to increase faster with undercooling than the peritectic forming elements (Ti, Zr, and Cr). At undercooling temperature of 100 K, almost all the eutectic alloys have doubled their supersaturation, while the peritectic alloys are not saturated in the solid solution phase yet.

C. *Ternary Systems*

The developed model can also be applied to predict the phase selection of ternary compounds (or compounds containing even more elements) in the undercooled melt assuming the nucleation process is limited by only one element for a given composition. In this subsection, we use the β-AlFeSi intermetallic phase ($Al_9Fe_2Si_2$) as an example to demonstrate the applicability of the developed model.

Al-Si alloys are one of the most widely used aluminum alloys especially in the automobile industry due to their excellent castability and good mechanical properties.[39,40] Al-Si-based alloys such as $AlSi_{10}Mg$ have also been adopted in AM thanks to their outstanding resistance to cracking. Due to the presence of impurity iron, which is a result of the Bayer refining process,[40] Al-Si alloys tend to form Al-Fe-Si ternary compounds. Among those complex compounds, the β-AlFeSi intermetallic phase is reported as one of the most deleterious phases in Al-Si alloys.[41] For instance, the formation of brittle β-AlFeSi due to high Fe contents in recycled alloys limits the use of secondary aluminum for structural components in the automotive industry. It was found that rates β-AlFeSi can be suppressed in casting by adding Mn and changing cooling.[42,43] However, the mechanism is still not well understood. In addition, the increased tolerance of impurity Fe in rapid solidification can significantly

Table I. Typical Values of Thermodynamics Property of α-Al and Intermetallic Phases from Thermo-Calc (TCAL7), Pandat (PanAl), and Al-Ta Database[37]

Phase	Entropy of fusion, ΔS_m ($Jmol^{-1}$ K^{-1})	Melting Temperature, T_M (K)	Density, ρ (g/cm^3)
α-Al	11.47	933.47	2.70
$Al_{45}Cr_7$	18.13	1203.56	3.22
Al_6Mn	15.62	1111.95	3.32
$Al_{12}Mn$	15.62	992.44	3.02
Al_3Zr ($D0_{23}$)	15.52	1892.32	4.17
$Al_3Ti(D0_{22})$	13.74	1669.07	3.36
$Al_3Sc(D0_{22})$	15.57	1477.81	3.03
$Al_{13}Fe_4$	17.16	1427.85	3.84
Al_3Ta	17.90	1814.51	6.85
$Al_9Fe_2Si_2$	15.59	1089.07	3.69

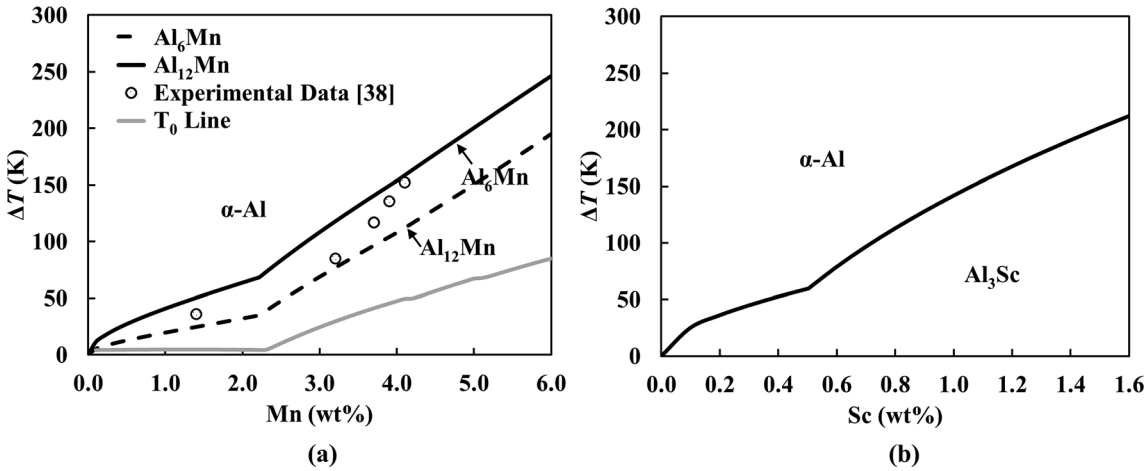

Fig. 2—(*a*) Critical undercooling of the competing phase in Al-Mn binary system, (*b*) Critical undercooling of the six competing phase in Al-Sc binary system.

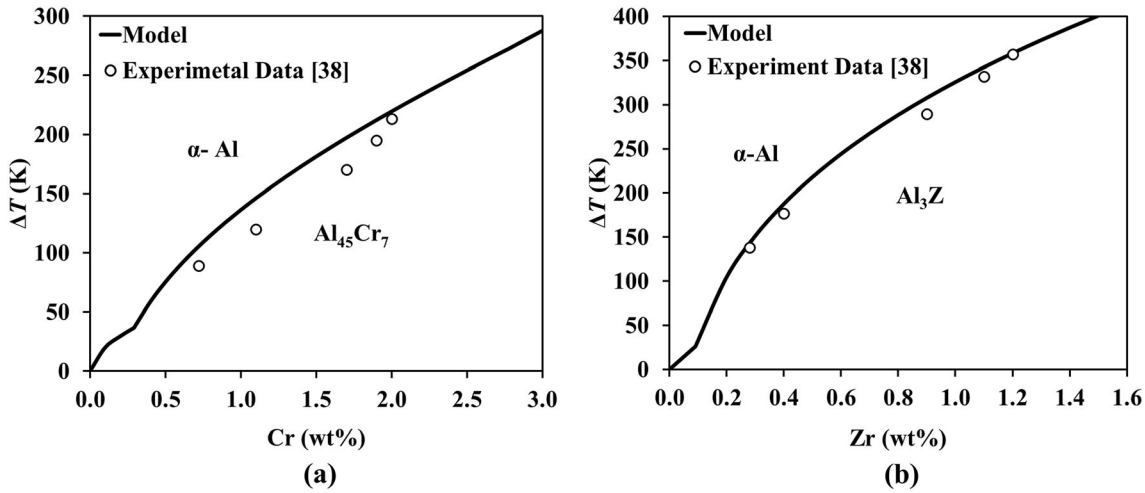

Fig. 3—(*a*) Critical undercooling of the competing phase in Al-Cr binary system, (*b*) Critical undercooling of the competing phase in Al-Zr binary system.

reduce the raw material cost for AM processes and improve the reusability of AM powders. Therefore, it is crucial to understand the phase stability for different undercoolings and extended solubility of Fe in Al-Si-Fe alloys for both recycling aluminum alloys and AM. Although several researchers have worked on the

Al-Fe-Si ternary system,[41,44] none of them have explored the dependence of phase selection on undercooling.

To simulate the competing nucleation of the ternary β-AlFeSi phase and the matrix α-Al phase, we assume the slower diffuser (Fe in this system) is the limiting element. Therefore, although the model is developed for binary, it can be extended to ternary and multicomponent phases. By applying Eq. [5], we calculated the phase selection diagram of β-AlFeSi and α-Al phase as a function of undercooling. It can be seen from the contour plot [Figure 5(a)] that the undercooling required to suppress the nucleation of β-AlFeSi shows different dependence on Fe and Si. The required undercooling increases dramatically with Fe, while it slowly decreases with the increasing Si concentration. Hence, for a given undercooling, increasing the Si content can increase the impurity tolerance of Fe. Our calculation also indicates that even a small undercooling can effectively suppress the formation of β-AlFeSi. For instance, for an undercooling of 100 K, the Fe concentration can reach as high as 5 wt pct.

Additionally, the nucleation may also be limited by the scarcest species (Fe or Si depending on the given composition). As shown in the calculated diagram in Figure 5(b), in the region above the dashed line, the nucleation is limited by Si concentration as it is less than Fe. Under the dashed line, the nucleation is limited by Fe concentration, which is the same as Figure 5(a). However, experiments are needed to validate the models for ternary systems. The applicability of the model to quaternary and multicomponent alloy system needs further investigation.

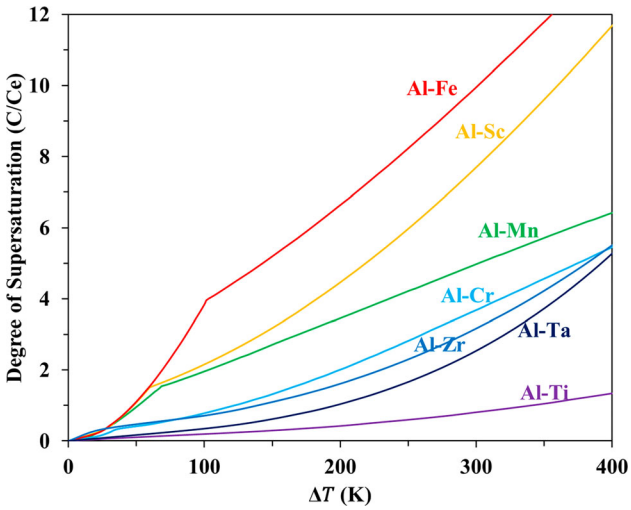

Fig. 4—Degree of supersaturation (c/c_e) as a function of undercooling (ΔT) for Fe, Sc, Mn, Cr, Zr, Ta, and Ti.

D. *Precipitation Strengthening*

One of the current directions of Al alloy development is the creep-resistant Al alloys for elevated temperature applications. Developing Al alloys to replace Ti alloys or superalloys for applications of around 300 °C may dramatically reduce the material and related processing costs. To achieve creep resistance at elevated temperatures, a large volume fraction of coherent precipitate phases is required. For instance, nickel-based superalloys that can withstand temperatures exceeding 75 pct of their melting point contain a high-volume fraction ($f \geq 0.5$) of precipitation phase $\gamma\prime$, which is coherent with the matrix phase γ. According to the investigations by Knipling *et al.*,[45] Al_3M phase ($L1_2$ structure) formers, such as Ti, Hf, Zr, and Sc, are found to be the best candidates for developing creep-resistant Al alloys. However, the biggest hurdle for developing such types of Al alloys is their limited solubilities. For example, Ti, Zr, and Hf have liquid solubility less than 0.01 at. pct, which significantly restricts the volume fraction of strengthening Al_3M phase one can achieve by casting.

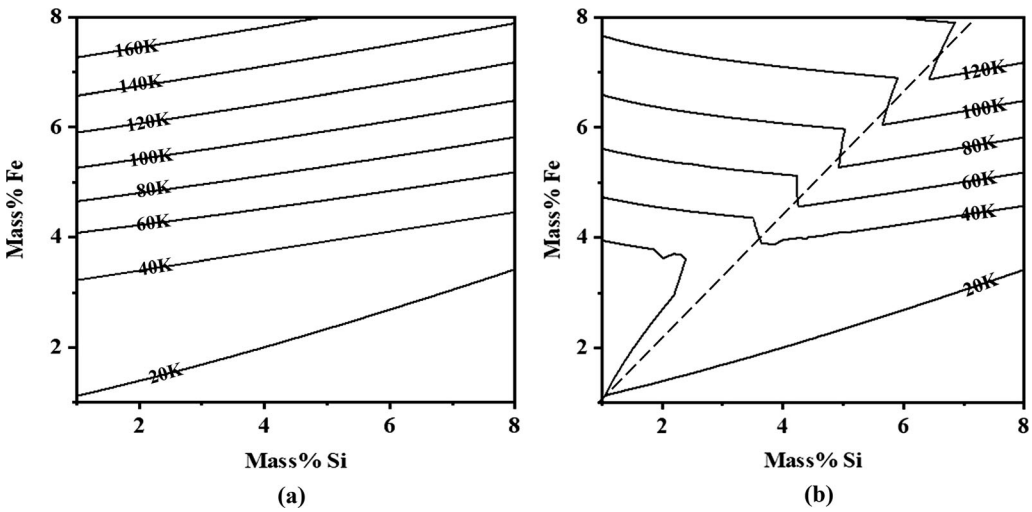

Fig. 5—Calculated critical undercooling as a function of Fe and Si concentration (wt pct) by assuming the nucleation is limited by (*a*) slower diffuser (Fe) or limited by (*b*) scarcest species. The dashed line indicates the change of limiting elements.

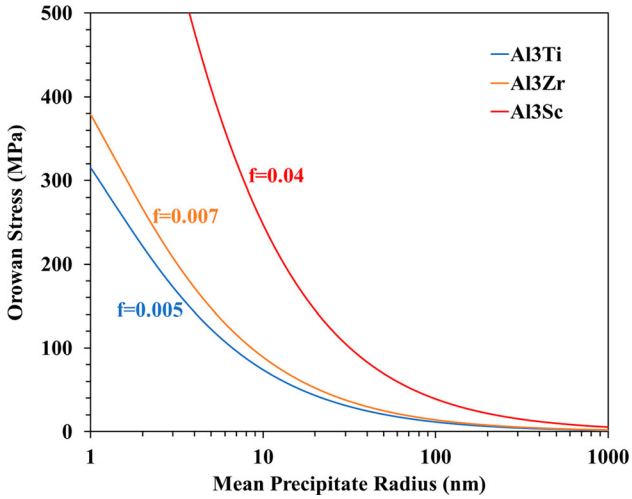

Fig. 6—The Orowan stress as a function of the mean precipitate radius for various volume fraction for dispersed phases.

Since rapid solidifications can significantly extend the solubility, we apply 200 K undercooling to see how strong the Al alloys may become using those Al_3M phase formers. By applying the model, we found the volume fraction of Al_3M phases that may form under 200 K undercooling is 0.04, 0.007, and 0.005 for Sc, Ti, and Zr, respectively. To evaluate the creep resistance, we calculate the Orowan stress[46] as a function of the size of the precipitate phase. The formula for calculating Orowan stress and the parameters can be found in the literature.[45] As shown in Figure 6, for the precipitates of 10 nm in radius, the Orowan stress for Al_3Sc ($f = 0.04$) is about 250 MPa, comparable to the yield strength of AA6061. Even for Al_3Ti ($f = 0.007$) and Al_3Zr ($f = 0.005$) the calculated Orowan stresses are nearly 100 MPa if the precipitate can be controlled to be around 10 nm in radius. Hence, in rapid solidification processes such as AM, the creep resistance can be dramatically improved by incorporating those elements. It should be noted that the resistance to coarsening is also critical for elevated temperature applications. It was found that the diffusivity of Ti and Zr at 400 °C are on the magnitude of 10^{-21} and 10^{-20} m^2 s^{-1},[45] indicating strong resistance to coarsening. Even for Sc, which has a diffusivity on the magnitude of 10^{-17} m^2 s^{-1} at 400 °C, recent studies have shown remarkably high coarsening and creep resistance at 300 °C.[47–49] Therefore, rapid solidification promises a new route for developing novel creep-resistant Al alloys by extending the solubility of Al_3M forming elements to achieve a high-volume fraction of strengthening precipitate phases.

IV. CONCLUSIONS

In this work, the phase selection model based on the time-dependent nucleation theory was modified to eliminate the dependence on diffusivity. The parameters needed by the new model can be easily accessed from CALPHAD packages and the physical property (density) database, which significantly improved the applicability and reliability of the model. The new model was applied to predict the extended solubility as a function of undercooling for various binary Al alloys. The predictions show good agreement with experiments. The T_0 line method, which is purely based on thermodynamics, neglected the kinetics of nucleation and hence overpredicts the solubilities. We demonstrated that the new model is also applicable to ternary and multicomponent phases, the solubility of which has never been theoretically studied before. This is very important since real alloys typically contain more than three elements. Lastly, the model was used to explore the possibility of developing creep-resistant Al alloys. It was found that 200 °C undercooling is sufficient to achieve decent high temperature strength by extending the solubility of Al_3M phase formers such as Ti, Zr, and Sc. This simple analytical model can be easily adopted for analyzing the phase selection in rapid solidification experiments. It will also shed light on new alloy designs for rapid solidification processes like AM.

ACKNOWLEDGMENTS

The authors would like to thank the Senior Design team, K. Duncan, J. B. Fletcher, C. Simcoe, E. Klafehn, and H. Long, for practicing the model, experimental trials, and helpful discussions.

CONFLICT OF INTEREST

On behalf of all authors, the corresponding author states that there is no conflict of interest.

APPENDIX

In the following, we use Al-Cr binary system as an example to illustrate how to obtain the relationship between extended solid solubility and undercooling.

1. Identifying the first intermetallic phase ($Al_{45}Cr_7$) appearing in the Al-rich side of the equilibrium Al-Cr binary phase diagram.
2. Calculating d_a of both $Al_{45}Cr_7$ and α-Al from the density data[36] using Eq. [2].
3. Evaluating the melting temperature T_M and molar entropy of fusion ΔS_m for both $Al_{45}Cr_7$ and α-Al using Thermo-Calc. To simplify, we assume Al-x wt pct Cr has the same melting temperature and entropy as pure Al. For low solute concentration, it is an acceptable assumption.
4. For each solubility value x, evaluating $x_{L,eff}$, *i.e.*, $x_{L,1} \approx 1.0$ (for small x), and $x_{L,2} = \frac{7x}{52}$.
5. Substituting all the parameters in and solving Eq. [5] to obtain the critical temperature T.
6. Calculating undercooling corresponding ΔT for each solubility value x, using the liquidus temperature of Al-x wt pct Cr obtained from Thermo-Calc (with database TCAL7).

REFERENCES

1. W.E. Frazier: Metal additive manufacturing: a review. *J. Mater. Eng. Perform.*, 2014, vol. 23, pp. 1917–28. https://doi.org/10.1007/s11665-014-0958-z.
2. D. Herlach: Non-equilibrium solidification of undercooled metallic metls. *Mater. Sci. Eng. R. Rep.*, 1994, vol. 12, pp. 177–272. https://doi.org/10.1016/0927-796X(94)90011-6.
3. H. Jones: The status of rapid solidification of alloys in research and application. *J. Mater. Sci.*, 1984, vol. 19, pp. 1043–76. https://doi.org/10.1007/BF01120015.
4. F.H. Froes, Y.-W. Kim, and S. Krishnamurthy: Rapid solidification of lightweight metal alloys. *Mater. Sci. Eng. A*, 1989, vol. 117, pp. 19–32. https://doi.org/10.1016/0921-5093(89)90082-8.
5. D. Herlach: Non-equilibrium solidification of undercooled metallic melts. *Metals (Basel)*, 2014, vol. 4, pp. 196–234. https://doi.org/10.3390/met4020196.
6. K. Eckler, D.M. Herlach, R.G. Hamerton, and A.L. Greer: Dendrite growth velocities in highly undercooled, dilute Ni-C melts. *Mater. Sci. Eng. A*, 1991, vol. 133, pp. 730–33. https://doi.org/10.1016/0921-5093(91)90173-K.
7. K. Eckler, R.F. Cochrane, D.M. Herlach, B. Feuerbacher, and M. Jurisch: Evidence for a transition from diffusion-controlled to thermally controlled solidification in metallic alloys. *Phys. Rev. B*, 1992, vol. 45, pp. 5019–22. https://doi.org/10.1103/PhysRevB.45.5019.
8. K. Eckler, A.F. Norman, F. Gärtner, A.L. Greer, and D.M. Herlach: Microstructures of dilute Ni C alloys obtained from undercooled droplets. *J. Cryst. Growth*, 1997, vol. 173, pp. 528–40. https://doi.org/10.1016/S0022-0248(96)01066-4.
9. K. Eckler and D. Herlach: Measurements of dendrite growth velocities in undercooled pure Ni-melts—some new results. *Mater. Sci. Eng. A*, 1994, vol. 178, pp. 159–62. https://doi.org/10.1016/0921-5093(94)90535-5.
10. Y. Wu, T.J. Piccone, Y. Shiohara, and M.C. Flemings: Dendritic growth of undercooled nickel-tin: Part I. *Metall. Trans. A*, 1987, vol. 18, pp. 915–24. https://doi.org/10.1007/BF02646933.
11. Y. Wu, T.J. Piccone, Y. Shiohara, and M.C. Flemings: Dendritic growth of undercooled nickel-tin: Part II. *Metall. Mater. Trans. A*, 1987, vol. 18, pp. 925–32. https://doi.org/10.1007/BF02646934.
12. Y. Wu, T.J. Piccone, Y. Shiohara, and M.C. Flemings: Dendritic growth of undercooled nickel-tin: Part III. *Metall. Trans. A*, 1988, vol. 19, pp. 1109–19. https://doi.org/10.1007/BF02628395.
13. A. Munitz, A.B. Gokhale, and R. Abbaschian: Effect of supercooling on the microstructure of Al-Nb alloys. *J. Mater. Sci.*, 2000, vol. 35, pp. 2263–71. https://doi.org/10.1023/A:1004783011253.
14. N.J.E. Adkins, N. Saunders, and P. Tsakiropoulos: Rapid solidification of peritectic aluminium alloys. *Mater. Sci. Eng.*, 1988, vol. 98, pp. 217–19. https://doi.org/10.1016/0025-5416(88)90158-9.
15. M.G. Chu, A. Giron, and D.A. Granger: Microstructure and heat flow in melt-spun aluminum alloys, in *Proc. ASM's Int. Conf. Rapidly Solidified Mater., Metals Park, OH*, 1986, pp. 311–16.
16. M.G. Chu and D.A. Granger: Solidification and microstructure analysis of rapidly solidified melt-spun Al-Fe alloys. *Metall. Trans. A*, 1990, vol. 21, pp. 205–12. https://doi.org/10.1007/BF02656437.
17. G. Waterloo and H. Jones: Microstructure and thermal stability of melt-spun Al-Nd and Al-Ce alloy ribbons. *J. Mater. Sci.*, 1996, vol. 31, pp. 2301–10. https://doi.org/10.1007/BF01152938.
18. J. Xu, Q. Zhou, J. Kong, Y. Peng, S. Guo, J. Zhu, and J. Fan: Solidification behavior and microstructure of Ti-(37–52) at% Al alloys synthesized in situ via dual-wire electron beam freeform fabrication. *Addit. Manuf.*, 2021, https://doi.org/10.1016/j.addma.2021.1021139.
19. Q. Tan, Y. Yin, A. Prasad, G. Li, Q. Zhu, D.H. StJohn, and M.X. Zhang: Demonstrating the roles of solute and nucleant in grain refinement of additively manufactured aluminium alloys. *Addit. Manuf.*, 2022, https://doi.org/10.1016/j.addma.2021.102516.
20. M. Opprecht, J.-P. Garandet, G. Roux, and C. Flament: An understanding of duplex microstructures encountered during high strength aluminium alloy laser beam melting processing. *Acta Mater.*, 2021, vol. 215, p. 117024. https://doi.org/10.1016/j.actamat.2021.117024.
21. F. Xiao, S. Wang, Y. Wang, D. Shu, G. Zhu, B. Sun, and D. StJohn: Niobium nanoparticle-enabled grain refinement of a crack-free high strength Al-Zn-Mg-Cu alloy manufactured by selective laser melting. *J. Alloys Compd.*, 2022, vol. 900, p. 163427. https://doi.org/10.1016/j.jallcom.2021.163427.
22. Y. Wang, X. Lin, N. Kang, Z. Wang, Q. Wang, Y. Liu, and W. Huang: Laser powder bed fusion of Zr-modified Al–Cu–Mg alloy: crack-inhibiting, grain refinement, and mechanical properties. *Mater. Sci. Eng. A*, 2022, vol. 838, p. 142618. https://doi.org/10.1016/j.msea.2022.142618.
23. Z. Wang, X. Lin, Y. Tang, N. Kang, X. Gao, S. Shi, and W. Huang: Laser-based directed energy deposition of novel Sc/Zr-modified Al-Mg alloys: columnar-to-equiaxed transition and aging hardening behavior. *J. Mater. Sci. Technol.*, 2021, vol. 69, pp. 168–79. https://doi.org/10.1016/j.jmst.2020.08.003.
24. Q. Li, G. Li, X. Lin, D. Zhu, J. Jiang, S. Shi, F. Liu, W. Huang, and K. Vanmeensel: Development of a high strength Zr/Sc/Hf-modified Al-Mn-Mg alloy using Laser Powder Bed Fusion: design of a heterogeneous microstructure incorporating synergistic multiple strengthening mechanisms. *Addit. Manuf.*, 2022, vol. 57, p. 102967. https://doi.org/10.1016/j.addma.2022.102967.
25. Z. Wang, X. Lin, N. Kang, J. Chen, H. Tan, Z. Feng, Z. Qin, H. Yang, and W. Huang: Laser powder bed fusion of high-strength Sc/Zr-modified Al–Mg alloy: phase selection, microstructural/mechanical heterogeneity, and tensile deformation behavior. *J. Mater. Sci. Technol.*, 2021, vol. 95, pp. 40–56. https://doi.org/10.1016/j.jmst.2021.03.069.
26. Z. Wang, X. Lin, L. Wang, Y. Cao, Y. Zhou, and W. Huang: Microstructure evolution and mechanical properties of the wire + arc additive manufacturing Al-Cu alloy. *Addit. Manuf.*, 2021, vol. 47, p. 102298. https://doi.org/10.1016/j.addma.2021.102298.
27. M. Asta, C. Beckermann, A. Karma, W. Kurz, R. Napolitano, M. Plapp, G. Purdy, M. Rappaz, and R. Trivedi: Solidification microstructures and solid-state parallels: recent developments, future directions. *Acta Mater.*, 2009, vol. 57, pp. 941–71. https://doi.org/10.1016/j.actamat.2008.10.020.
28. W. Kurz, M. Rappaz, and R. Trivedi: Progress in modelling solidification microstructures in metals and alloys. Part II: dendrites from 2001 to 2018. *Int. Mater. Rev.*, 2021, vol. 66, pp. 30–76. https://doi.org/10.1080/09506608.2020.1757894.
29. P.K. Galenko and D. Jou: Rapid solidification as non-ergodic phenomenon. *Phys. Rep.*, 2019, vol. 818, pp. 1–70. https://doi.org/10.1016/j.physrep.2019.06.002.
30. J.C. Baker and J.W. Cahn: Thermodynamics of solidification, in *The Selected Works of John W. Cahn*. Wiley, Hoboken, 2013, pp. 253–88. https://doi.org/10.1002/9781118788295.ch26.
31. J.L. Murray: Thermodynamic factors in the extension of solid solubility in Al-based alloys. *MRS Proc.*, 1982, vol. 19, p. 249. https://doi.org/10.1557/PROC-19-249.
32. G. Shao and P. Tsakiropoulos: Prediction of phase selection in rapid solidification using time dependent nucleation theory. *Acta Metall. Mater.*, 1994, vol. 42, pp. 2937–42. https://doi.org/10.1016/0956-7151(94)90391-3.
33. J.-O.O. Andersson, T. Helander, L. Höglund, P. Shi, and B. Sundman: Thermo-Calc & DICTRA, computational tools for materials science. *Calphad Comput. Coupling Phase Diagr. Thermochem.*, 2002, vol. 26, pp. 273–312. https://doi.org/10.1016/S0364-5916(02)00037-8.
34. W. Cao, S.-L.L. Chen, F. Zhang, K. Wu, Y. Yang, Y.A.A. Chang, R. Schmid-Fetzer, and W.A.A. Oates: PANDAT software with PanEngine, PanOptimizer and PanPrecipitation for multi-component phase diagram calculation and materials property simulation. *Calphad Comput. Coupling Phase Diagr. Thermochem.*, 2009, vol. 33, pp. 328–42. https://doi.org/10.1016/j.calphad.2008.08.004.
35. J.A. Cahill and A.V. Grosse: Viscosity and self-diffusion of liquid thallium from its melting point to about 1300°K. *J. Phys. Chem.*, 1965, vol. 69, pp. 518–21. https://doi.org/10.1021/j100886a026.
36. https://materials.springer.com/. (n.d.).
37. V.T. Witusiewicz, A.A. Bondar, U. Hecht, J. Zollinger, V.M. Petyukh, O.S. Fomichov, V.M. Voblikov, and S. Rex: Experimental study and thermodynamic re-assessment of the binary Al-Ta system. *Intermetallics*, 2010, vol. 18, pp. 92–106. https://doi.org/10.1016/j.intermet.2009.06.015.
38. R. Ichikawa, T. Ohashi, and T. Ikeda: Effects of cooling rate and supercooling degree on solidified structure of Al-Mn, Al-Cr and Al-Zr in rapid solidification. *Trans. Jpn. Inst. Met.*, 1971, vol. 12, pp. 280–84.

39. L.Y. Zhang, Y.H. Jiang, Z. Ma, S.F. Shan, Y.Z. Jia, C.Z. Fan, and W.K. Wang: Effect of cooling rate on solidified microstructure and mechanical properties of aluminium-A356 alloy. *J. Mater. Process. Technol.*, 2008, vol. 207, pp. 107–11. https://doi.org/10.1016/j.jmatprotec.2007.12.059.
40. J.A. Taylor: Iron-containing intermetallic phases in Al-Si based casting alloys. *Procedia Mater. Sci.*, 2012, vol. 1, pp. 19–33. https://doi.org/10.1016/j.mspro.2012.06.004.
41. W.S. Ebhota and T.-C. Jen: Intermetallics formation and their effect on mechanical properties of Al-Si-X alloys, in *Intermetallic Compounds—Formation and Applications*. InTech, London, 2018. https://doi.org/10.5772/intechopen.73188.
42. E. Cinkilic, C.D. Ridgeway, X. Yan, and A.A. Luo: A formation map of iron-containing intermetallic phases in recycled cast aluminum alloys. *Metall. Mater. Trans. A*, 2019, vol. 50, pp. 5945–56. https://doi.org/10.1007/s11661-019-05469-6.
43. E. Cinkilic, M. Moodispaw, J. Zhang, J. Miao, and A.A. Luo: A new recycled Al–Si–Mg alloy for sustainable structural die casting applications. *Metall. Mater. Trans. A*, 2022, vol. 53, pp. 2861–73. https://doi.org/10.1007/s11661-022-06711-4.
44. M. Yıldırım and D. Özyürek: The effects of Mg amount on the microstructure and mechanical properties of Al–Si–Mg alloys. *Mater. Des.*, 2013, vol. 51, pp. 767–74. https://doi.org/10.1016/j.matdes.2013.04.089.
45. K.E. Knipling, D.C. Dunand, and D.N. Seidman: Criteria for developing castable, creep-resistant aluminum-based alloys—a review. *Zeitschrift Für Met.*, 2006, vol. 97, pp. 246–65. https://doi.org/10.3139/146.101249.
46. J.F. Nie and B.C. Muddle: Microstructural design of high-strength aluminum alloys. *J. Phase Equilib.*, 1998, vol. 19, pp. 543–51. https://doi.org/10.1361/105497198770341734.
47. M.E. van Dalen, D.C. Dunand, and D.N. Seidman: Effects of Ti additions on the nanostructure and creep properties of precipitation-strengthened Al–Sc alloys. *Acta Mater.*, 2005, vol. 53, pp. 4225–35. https://doi.org/10.1016/j.actamat.2005.05.022.
48. D.N. Seidman, E.A. Marquis, and D.C. Dunand: Precipitation strengthening at ambient and elevated temperatures of heat-treatable Al(Sc) alloys. *Acta Mater.*, 2002, vol. 50, pp. 4021–35. https://doi.org/10.1016/S1359-6454(02)00201-X.
49. E. Marquis, D. Seidman, M. Asta, and C. Woodward: Composition evolution of nanoscale AlSc precipitates in an Al–Mg–Sc alloy: experiments and computations. *Acta Mater.*, 2006, vol. 54, pp. 119–30. https://doi.org/10.1016/j.actamat.2005.08.035.